Mineralogy and Petrology (2024) 118:89–103
https://doi.org/10.1007/s00710-023-00848-9

RESEARCH

The auriferous quartz lode of the Veloso deposit, Quadrilátero Ferrífero of Minas Gerais, Brazil: geological characterisation and constraints from tourmaline boron isotopes

Júlia S. Pimenta[1] · Alexandre R. Cabral[2] · Glaucia Queiroga[1] · Cristiano Lana[1] · Miguel Tupinambá[3] · Armin Zeh[4] · Rogerio Kwitko-Ribeiro[5]

Received: 4 February 2022 / Accepted: 4 November 2023 / Published online: 28 November 2023

Abstract

Veloso is one of numerous and poorly documented auriferous deposits of Ouro Preto, the town that symbolises the gold rush in Brazil at the turn of the seventeenth century. We present the results of underground geological mapping, combined with a boron (B) isotopic study of tourmaline, an elusive mineral in the auriferous quartz lode of the historical Veloso deposit. Its lode is characteristically brecciated in a host rock that shows no cataclastic fabric. The host rock is itabirite, a metamorphosed banded iron formation. Tourmaline is essentially dravite and locally occurs as abundant crystals in breccia-cementing pockets of goethite, formed from the oxidation of sulfide minerals. Gold is spatially associated with tourmaline in the goethite-rich pockets. In situ measurements for B isotopes yielded $\delta^{11}B$ values in the range of −21 to −9‰. This range is similar to that reported for tourmaline of the Passagem de Mariana deposit, the best documented auriferous lode deposit at the south-eastern edge of the Quadrilátero Ferrífero. The tourmaline B isotopic data reflect auriferous fluids of crustal origin that sourced B from metasedimentary rocks, which may include a non-marine evaporitic component.

Keywords Veloso gold deposit · Tourmaline boron isotopes · Mariana anticline · Quadrilátero Ferrífero · Minas Gerais

Introduction

Ouro Preto is the symbol of the gold rush in Brazil, which started at the end of the seventeenth century, to the highlands of a region that became known as Minas Gerais – i.e., the province of the general mines. The gold deposits of the Ouro Preto area are thought to either differ from conventional orogenic (mesothermal) gold deposits in that they formed during late-orogenic collapse tectonics, as advanced by Chauvet et al. (2001), or represent orogenic gold deposits, as proposed for the Passagem de Mariana lode by Vial et al. (2007), following the definition of Groves et al. (1998). However, apart from one large gold deposit, the Passagem de Mariana lode, which has extensively been investigated (Eschwege 1833; Ferrand 1894; Hussak 1898; Derby 1911; Fleischer and Routhier 1973; Ladeira 1988; Chauvet et al. 2001; Cavalcanti and Xavier 2006; Vial et al. 2007; Cabral and Zeh 2015b; Trumbull et al. 2019), and cited in classical textbooks (e.g., Lindgren 1933, Emmons 1940), little is known about other gold deposits in the Ouro Preto area.

Editorial handling: C. Hauzenberger

✉ Júlia S. Pimenta
juliaspim@gmail.com

[1] Departamento de Geologia (Degeo), Universidade Federal de Ouro Preto (UFOP), Campus Morro do Cruzeiro s/n, Ouro Preto, MG 35400-000, Brazil

[2] Programa de Pós-Graduação em Evolução Crustal e Recursos Naturais, Universidade Federal de Ouro Preto (UFOP), Ouro Preto, MG 35400-000, Brazil

[3] Faculdade de geologia, Instituto Nacional de Ciência e Tecnologia GeoAtlantico, Tektos-Geotectonic Research Group, Universidade do Estado do Rio de Janeiro, Rio Janeiro-RJ 20550-050, Brazil

[4] Institut für Angewandte Geowissenschaften – Mineralogie und Petrologie, Karlsruher Institut für Technologie (KIT), Adenauerring 20b, Geb. 50.40, 76131 Karlsruhe, Germany

[5] Centro de Desenvolvimento Mineral, Vale S.A, Rodovia BR 381, km 450, Santa Luzia, MG 33040-900, Brazil

Veloso is one of the numerous underground workings for gold in the Ouro Preto area (Eschwege 1833; Lacourt 1937), dating back to the first half of the nineteenth century. The Veloso deposit has again become accessible and it is currently a tourist site in the town of Ouro Preto (Fig. 1). In the course of detailed underground mapping, we recovered tourmaline from the Veloso auriferous quartz lode, where tourmaline is not obvious to the naked eye. In contrast, tourmaline is abundant at Passagem de Mariana, for which a B isotopic study has recently been published (Trumbull et al. 2019). Boron isotopic compositions of tourmaline are useful in distinguishing among different B reservoirs and, therefore, can assist in constraining the provenance of fluids that formed hydrothermal ore deposits (e.g., Slack et al. 1993; Trumbull et al. 2011; Mercadier et al. 2012; Büttner et al. 2016). Here, we provide background information on the Veloso auriferous lode, focussing on its tourmaline component, for which we present major-element and B isotopic compositions. We also present major- and minor-element compositions of the gold recovered from the quartz lode. Our data are compared with those from the Passagem de Mariana lode and then discussed in the geological context of the Mariana anticline.

Geological setting

The historical Veloso gold deposit is located in the southeastern portion of the Quadrilátero Ferrífero (Fig. 1), in the Mariana anticline. The latter is approximately 5 km wide and comprises two ridges, Serra de Ouro Preto and Serra de Antônio Pereira, on the southern and northern flanks, respectively. The core of the Mariana anticline encompasses rocks of the Rio das Velhas Supergroup, an Archaean greenstone-belt sequence, whereas the fold flanks show outcrops of the Minas Supergroup, which unconformably rests on the former (Dorr 1969). The Minas Supergroup is a dominantly clastic metasedimentary sequence with an economically important chemical metasedimentary unit, the Itabira iron formation of Harder and Chamberlin (1915), or the Cauê

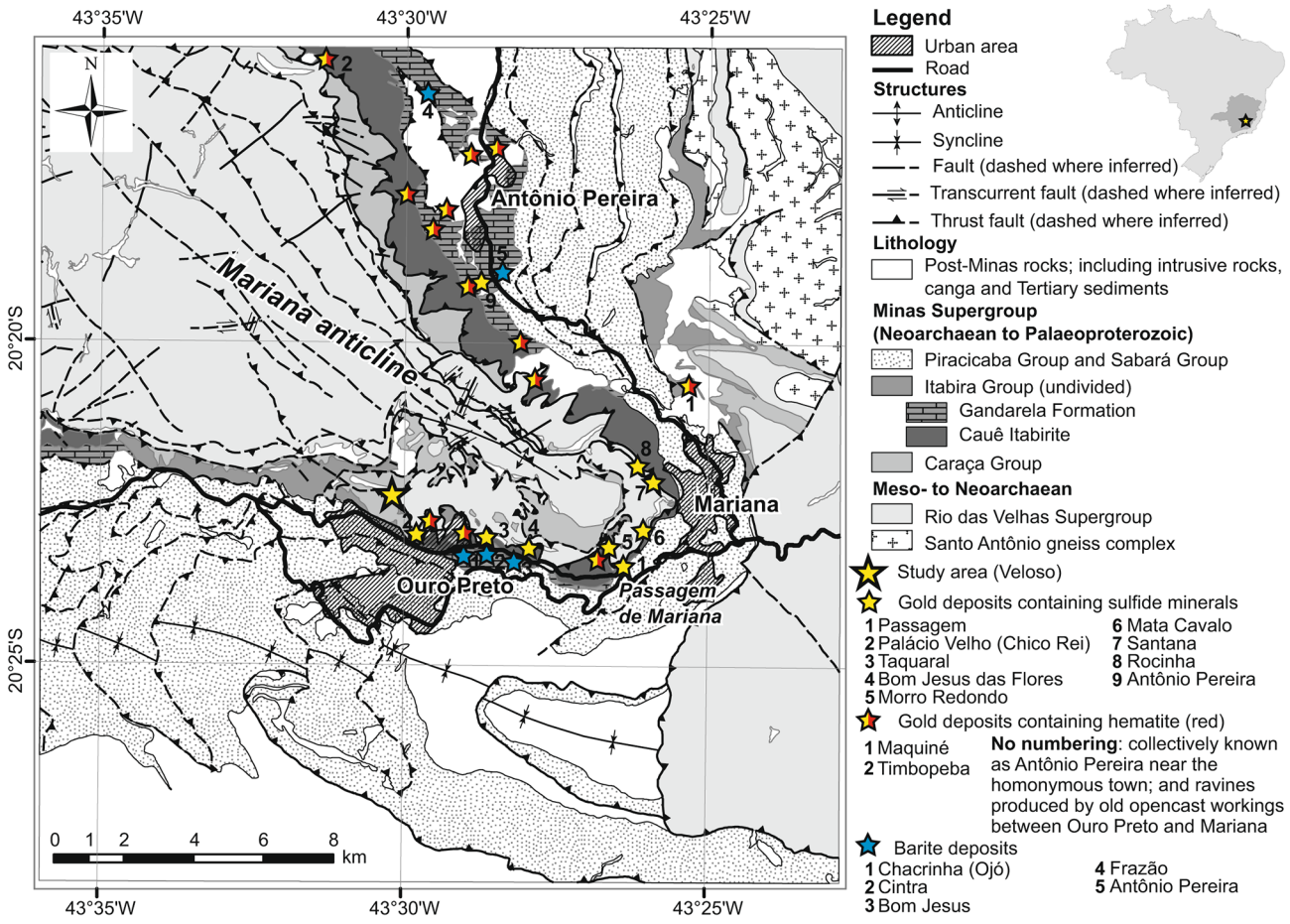

Fig. 1 Geological map of the Mariana anticline with emphasis on the mineral deposits (see Cabral et al. 2013 for references). Stars locate the main deposits in the region, which are divided into barite deposits (blue), hematite-rich auriferous deposits (red and yellow), and sulfide auriferous deposits (yellow). Veloso, the study area, is classified as a sulfide-bearing auriferous deposit

Itabirite of Dorr (1969), which hosts world-class iron-ore deposits. This unit also hosts the Veloso lode. Stratigraphic units of the Minas Supergroup that are pertinent to this study belong to the Caraça, the Itabira and the Piracicaba groups.

The basal unit of the Caraça Group has quartzite and minor metaconglomerate, making up the Moeda Formation, a unit that is locally interfingered with predominantly sericitic phyllite of the Batatal Formation (Wallace 1965; Dorr 1969). The latter, which also contains dolomitic intercalations (Fleischer and Routhier 1973), grades into the chemical sedimentary rocks of the Itabira Group, consisting mainly of itabirite and dolomitic rocks. Itabirite is a metamorphosed iron formation of alternating bands rich in hematite and/or magnetite, and in gangue minerals, mostly quartz. The itabirite unit, the Cauê Itabirite, passes gradually into the overlying dolomitic rocks of the Gandarela Formation. The depositional age of the Itabira Group is disputed. A Pb–Pb "isochron" age of 2.42 Ga for dolomitic rocks was proposed as the depositional age of the Itabira Group (Babinski et al. 1995), based on a poorly defined slope (MSWD = 187 – i.e., mean squared weighted deviation), whereas a U–Pb zircon age of 2.65 Ga for an itabirite-hosted metavolcanic layer was interpreted to reflect volcanism coeval with the deposition of Fe-rich sediments (Cabral et al. 2012c). The Itabira Group is overlain by the Piracicaba Group along an erosive unconformity. The basal unit of the Piracicaba Group, the Cercadinho Formation, consists of ferruginous quartzite and phyllite (Dorr 1969). The age of the erosive unconformity is constrained at ca. 2.18 Ga (Cabral and Zeh 2015a).

The Mariana anticline has been considered to result from two major tectonic events (Chemale et al. 1994; Alkmim and Marshak 1998): a Palaeoproterozoic orogenic event at ca. ~2.0 Ga, responsible for the regional folds and emplacement of gneissic domes of the Quadrilátero Ferrífero, and a Neoproterozoic thrust-and-fold event at ca. 0.6 Ga, the Brasiliano orogeny. On the other hand, some authors proposed that the main phase of regional folding and dome emplacement took place during the Brasiliano orogeny (Hippertt and Davis 2000). These models illustrate that the tectonic evolution of the Quadrilátero Ferrífero is disputed, but most authors agree that the pervasive foliation in the supracrustal rocks, particularly in the eastern part of the Quadrilátero Ferrífero, formed during the Brasiliano overprint (e.g., Chemale et al. 1994; Alkmim and Marshak 1998; Rosière et al. 2001; Hippertt and Davis 2000). The regional metamorphism reached greenschist-facies conditions in the Mariana anticline (Herz 1978).

A variety of mineral deposits occur in the Mariana anticline. Their distribution shows a redox sulfate–hematite–sulfide zoning (Fig. 1), given by barite deposits, hematite-rich gold deposits, and tourmaline–sulfide auriferous deposits, respectively (Cabral et al. 2013). The latter is typified by the Passagem de Mariana deposit, within the Batatal Formation of the Caraça Group (Fleischer and Routhier 1973; Vial et al. 2007). Passagem de Mariana is a quartz-lode deposit with carbonate minerals and ubiquitous tourmaline, and minor sulfide minerals, the most abundant of which is arsenopyrite (Vial et al. 2007). Graphite is present within the quartz lode (Oberthür and Weiser 2008; Cabral and Zeh 2015b). The lode-hosted sulfide minerals and graphite define Passagem de Mariana as a reduced member of the redox zoning of mineral deposits in the Mariana anticline. The oxidised counterpart consists of barite veins that cut the foliation of the host rock at low angle. This low-angle cross-cutting relationship between veins and host rocks is also observed in the Passagem de Mariana lode (Chauvet et al. 2001; Vial et al. 2007; Cabral et al. 2013), as well as in the Veloso lode (this study). Chauvet et al. (2001) have suggested that the Passagem de Mariana deposit formed in response to the tectonic collapse of the Brasiliano orogeny. A different view is found in Vial et al. (2007), who have temporally associated the Passagem de Mariana deposit with the Palaeoproterozoic event. Recent data, nevertheless, have favoured a late Brasiliano age – i.e., a concordant U–Pb age of 496.3 ± 2.0 Ma for xenotime crystals in a tourmaline pocket in the auriferous quartz lode of Passagem de Mariana (Cabral and Zeh 2015b). Several studies on gold and topaz deposits that are hosted in rocks of the Minas Supergroup have indicated a regional hydrothermal overprint at ca. 500 Ma (Cabral et al. 2015; Pereira et al. 2019; Gonçalves et al. 2019).

Materials and methods

Geological mapping of the underground mine was carried out at the scale of 1:100. The mapping followed a projection method, traditionally employed in the underground gold mines of Minas Gerais. The method consists in tangentially projecting points of geological elements, such as lithological contacts, using the plunge of the prominent lineation observed in the rocks, onto a horizontal plane (D. S. Vial, personal communication, 2019). The projection plane was set at 2 m above the floor.

A sample of the Veloso lode, VEL-04, was processed to concentrate heavy minerals at the Laboratório Geológico de Preparação de Amostras, located at the Universidade Estadual do Rio de Janeiro (UERJ). The sample was comminuted utilising a jaw crusher. Its heavy minerals were then concentrated by means of a Wilfley table. Further separation was performed through a heavy-liquid column of methylene iodide, followed by a Frantz isomagnetic separator of the < 177-μm fraction. Tourmaline grains, identified in the 0.3- and 0.4-A magnetic fractions, were manually picked and embedded in resin for

electron-probe microanalysis by wavelength-dispersive spectrometry (WDS), using a JXA-8230 JEOL electron microprobe (Table 1 and Supplementary Table S1), housed at the Microscopy and Microanalysis Laboratory (LMic), Universidade Federal de Ouro Preto (UFOP). The instrument was operated at 15 kV and 20 nA, with an electron-beam diameter of 5 μm (see Electronic Supplementary Material, ESM Table 1 for analytical details). Raw data were reduced online using a JEOL software that corrected all electron-probe microanalyses for background and ZAF parameters. Analytical errors are between 0.2 and 1.0%. Total Fe content is expressed as FeO. Calculation of tourmaline formulae, in atoms per formula unit (apfu), is based on 15 cations for the tetrahedral and octahedral sites, whereas contents of B_2O_3 were calculated for B = 3 apfu, according to stoichiometric constraints (Henry et al. 2011).

Another lode sample, VEL-06, was also crushed for concentrating heavy minerals. Its comminuted material was put through a Knelson gravity concentrator, housed at Centro de Desenvolvimento da Tecnologia Nuclear (CDTN, Belo Horizonte). After removing the magnetic fraction, an aliquot was further concentrated by heavy-liquid separation (bromoform). Gold grains, which were manually picked from a heavy-mineral concentrate, were first investigated by backscattered-electron imaging and energy-dispersive spectrometry (EDS), and then embedded in resin and polished for electron-probe microanalysis (Table 2). The JXA-8230 JEOL electron microprobe was employed in the WDS mode to analyse gold grains at 20 kV and 40 nA, with an electron-beam diameter of 2 μm (see ESM Table 1 for analytical details). Analytical errors are within 1%.

Where possible, electron-probe spot sites on tourmaline were analysed for B isotopes by means of a Thermo-Scientific Neptune Plus multi-collector ICP–MS, coupled to a Photon Machines 193 Excimer laser-ablation system at the UFOP. The method is described in Albert et al. (2018) and only a summary is provided here. Laser fluence was 5.29 J.cm^{-2} at a repetition rate of 15 Hz. Samples were ablated in a He atmosphere (0.8 L/min), which had a Helix ablation cell. Measurements for B isotopes were carried out in two sessions under the same analytical conditions. During the first session for B isotopes, the average standard deviation was 1.27‰ δ^{11}B and 18 analytical spots had a diameter of 25 μm, but 40 μm for 17 analytical spots. For the second session, 30 spots of 20-μm diameter yielded an average standard deviation of 0.27‰ δ^{11}B.

The data quality was tested using reference dravite (#108796, $\delta^{11}B = -6.6 \pm 0.1$‰; Dyar et al. 2001; Leeman and Tonarini 2001). External reference materials were elbaite (#98144, $\delta^{11}B = -10.4 \pm 0.2$‰; Dyar et al. 2001; Leeman and Tonarini 2001) and schorl (B4, $\delta^{11}B = -8.7 \pm 0.2$‰; Tonarini et al. 2003). Tourmaline schorl was employed as calibrant (#112566, $\delta^{11}B = -12.5 \pm 0.1$‰; Dyar et al. 2001; Leeman and Tonarini 2001). The correction factor applied to calculate the values of $^{11}B/^{10}B$ varied from 0.8841 to 0.8610. All measurements of reference materials are reported in ESM Table S1. Mineral abbreviations are those in Whitney and Evans (2010).

Results

Geology of the auriferous lode of Veloso

The Veloso auriferous lode is hosted in itabirite of the Cauê Itabirite (Fig. 2a,b). The main adit trends S–N for approximately 200 m, from the mine entrance to the currently accessible part. The host rock has a pervasive foliation, which gently dips towards SSE (~ 165°/26°). The layering is defined by the planar arrangement of specular-hematite-rich bands that alternate with quartz-rich bands. The auriferous mineralisation occurs as a quartz lode that is subconcordant with the host itabirite, truncating it at low angle. Where the main adit intercepts the quartz lode, the latter was mined along its strike, approximately E–W (Fig. 2a). The lode is extensively brecciated and oxidised (Fig. 2c), and pinches out laterally, reaching approximately 1 m in thickness (Fig. 2b), the projection equivalent of which on a horizontal reference plane is 2 m (Fig. 2a). The oxidised state of the quartz lode manifests itself as goethite-lined boxwork cavities. Sulfide minerals are generally absent, but arsenopyrite and pyrite can sporadically be observed in goethite-rich pockets, with and without scorodite (hydrated iron arsenate). Linear elements in the host itabirite, such as mineral lineation and fold axes, tend to be parallel to the dip direction of the itabirite layering.

It should be noticed that the main adit, close to the mine entrance, exposes a few layers of friable, foliated, clayey rock, concordant with the host itabirite. The thickness of such clayey layers reaches 1 dm (decimetre). The clayey rock, described in Cabral et al. (2020), represents a 620-m.y.-old intrusion that acquired its tectonic foliation during the Brasiliano orogeny. Those authors have used the magmatic rock, which now occurs as foliated sills in the itabirite sequence, to constrain the age of the Veloso lode as younger than 620 Ma (Cabral et al. 2020), as the lode truncates at low angle the layering of the host itabirite (Fig. 2a,b). The cross-cutting relationship between the lode and the host-rock layering is analogous to that of the Passagem de Mariana lode, for which an age of ca. 500 Ma has been determined (Cabral and Zeh 2015b). By analogy, we suggest that the age of the Veloso lode formed ca. 500 m.y. ago, a suggestion that is consistent with the age obtained for the regional hydrothermal overprint (Cabral et al. 2015; Pereira et al. 2019; Gonçalves et al. 2019).

Table 1 Representative B isotopic and major-element compositions of tourmaline from the Veloso lode

Spot number	5*	6*	8	19*	20*	24*	44	64*	65*	72	74	79	23*	1.27*	1.33*	2.03*	2.05*	2.13*
$\delta^{11}B$ (‰)	−10.02	−10.82	−9.51	−15.88	−15.39	−17.42	−11.29	−19.08	−14.04	−12.91	−8.81	−14.25	–	−12.50	−14.92	−15.03	−15.35	−15.11
± SD $\delta^{11}B$(‰)	1.27	1.27	1.27	0.27	0.27	0.27	1.27	1.27	1.27	1.27	1.27	0.27	–	1.27	1.85	0.27	0.27	0.27
B_2O_3 (%)	10.59	10.52	10.62	10.35	10.67	10.49	10.56	10.57	10.59	10.56	10.71	10.14	10.63	–	–	–	–	–
SiO_2	37.08	36.82	37.04	36.33	37.34	36.87	36.84	37.08	36.86	37.07	37.45	35.49	37.04	–	–	–	–	–
Al_2O_3	32.45	32.10	32.66	30.85	32.79	31.48	32.37	32.90	32.38	32.51	32.92	30.48	32.31	–	–	–	–	–
TiO_2	0.51	0.50	0.42	0.95	0.39	0.97	0.48	0.11	0.40	0.18	0.47	0.83	0.51	–	–	–	–	–
FeO (total)	3.91	3.93	3.64	8.71	3.97	6.91	3.97	4.45	3.88	4.31	4.04	9.78	3.94	–	–	–	–	–
Cr_2O_3	<0.06	<0.06	<0.06	<0.06	0.07	0.21	<0.06	<0.06	<0.06	0.07	<0.06	0.12	0.09	–	–	–	–	–
MnO	<0.05	<0.05	<0.05	<0.05	<0.05	<0.05	<0.05	<0.05	<0.05	<0.05	<0.05	<0.05	<0.05	–	–	–	–	–
MgO	8.33	8.36	8.54	5.82	8.39	6.75	8.34	7.76	8.59	8.04	8.36	4.87	8.69	–	–	–	–	–
CaO	0.57	0.61	0.56	0.28	0.45	0.25	0.57	0.19	0.54	0.21	0.55	0.43	0.60	–	–	–	–	–
Na_2O	1.79	1.94	1.91	2.37	1.78	2.37	1.98	1.54	2.01	1.59	1.96	1.90	1.82	–	–	–	–	–
K_2O	<0.02	<0.02	<0.02	0.03	<0.02	0.05	<0.02	<0.02	<0.02	<0.02	<0.02	0.17	<0.02	–	–	–	–	–
F	0.26	0.39	0.15	<0.13	0.23	0.19	0.27	<0.13	0.15	0.18	0.17	<0.13	0.21	–	–	–	–	–
	95.49	95.16	95.53	95.69	96.09	96.55	95.37	94.62	95.40	94.69	96.61	94.20	95.83	–	–	–	–	–
F–O	0.11	0.16	0.06	0.00	0.10	0.08	0.11	0.01	0.06	0.07	0.07	0.00	0.09	–	–	–	–	–
Total	95.38	95.00	95.47	95.69	95.99	96.47	95.26	94.61	95.34	94.62	96.54	94.20	95.74	–	–	–	–	–
apfu																		
Si	6.085	6.085	6.063	6.099	6.081	6.107	6.066	6.096	6.051	6.104	6.078	6.085	6.055	–	–	–	–	–
Al	6.276	6.251	6.302	6.104	6.294	6.146	6.280	6.376	6.264	6.308	6.296	6.161	6.226	–	–	–	–	–
Mg	2.039	2.059	2.084	1.455	2.037	1.668	2.048	1.902	2.103	1.973	2.022	1.245	2.118	–	–	–	–	–
Fe	0.537	0.543	0.498	1.222	0.541	0.958	0.547	0.612	0.533	0.593	0.548	1.402	0.538	–	–	–	–	–
Cr					0.010	0.027				0.009		0.016	0.011	–	–	–	–	–
Ti	0.063	0.063	0.052	0.120	0.047	0.121	0.059	0.014	0.049	0.022	0.057	0.107	0.063	–	–	–	–	–
Ca	0.100	0.108	0.099	0.051	0.079	0.043	0.100	0.033	0.095	0.037	0.096	0.079	0.106	–	–	–	–	–
Na	0.570	0.623	0.605	0.772	0.563	0.762	0.632	0.491	0.638	0.508	0.616	0.632	0.575	–	–	–	–	–
K				0.007		0.010						0.038		–	–	–	–	–
Ca/(Ca + Na)	0.15	0.15	0.14	0.06	0.12	0.05	0.14	0.06	0.13	0.07	0.14	0.11	0.16	–	–	–	–	–
Mg/(Mg + Fe)	0.79	0.79	0.81	0.54	0.79	0.64	0.79	0.76	0.80	0.77	0.79	0.47	0.80	–	–	–	–	–
$^{X}\square/(^{X}\square+Na)$	0.37	0.30	0.33	0.18	0.39	0.19	0.30	0.49	0.29	0.47	0.32	0.28	0.36	–	–	–	–	–
Vacancy ($^{X}\square$)	0.33	0.27	0.30	0.17	0.36	0.18	0.27	0.48	0.27	0.46	0.29	0.25	0.32	–	–	–	–	–

SD of 1.27‰ and 0.27‰ stands for average standard deviation of the first and second analytical sessions, respectively. Asterisks correspond to analytical spots shown in Fig. 4

Total Fe content is expressed as FeO. Atoms per formula unit (apfu) is based on 15 cations for the tetrahedral and octahedral sites. B_2O_3 is calculated for B = 3 apfu, according to stoichiometric constraints

Tourmaline was not noticed in the lode during the underground mapping, but recovered from a heavy-mineral concentrate of a goethite-rich pocket of the brecciated lode (sample VEL-04). However, tourmaline was known from the early open-cast workings, where the mineral was recognised in the "carvoeira" underneath the itabirite sequence (Eschwege 1833). Eschwege (1833) defined the so-called "carvoeira" as friable tourmalinite containing manganese oxide – i.e., "ein mürbes Schörlgestein mit Mangan" (Eschwege 1833, p. 291). Eschwege (1833) further remarked that gold was sometimes so abundant that it became visible in the black mass of "carvoeira". Although "carvoeira" is no longer accessible at Veloso, the spatial connection of tourmaline with gold is highlighted by the finding of tourmaline inclusions in goethite-bearing gold grains (Fig. 3a, b). Such a spatial association makes the study of the composition and origin of tourmaline relevant to the understanding of gold mineralisation in the Mariana anticline.

Importantly, a recently collected sample from the Veloso lode, subsequent to the acquisition of the analytical data on which this work is based, depicts a spatial association between gold and tourmaline concentrations. Tourmaline is locally concentrated as breccia cement, binding vein-quartz fragments together (Fig. 3c). This breccia-cementing tourmaline occurs with muscovite laths within a goethite-rich groundmass where gold is located (Fig. 3c). The goethite-rich groundmass of Fig. 3c is analogous to the goethite-rich pocket from which tourmaline was recovered from a heavy-mineral concentrate (sample VEL-04). All analytical data come from the latter tourmaline, which represents the breccia-cementing tourmaline with which gold is spatially associated.

Chemical composition of gold

Quantitative electron-probe microanalysis of gold grains, obtained from a heavy-mineral concentrate of the brecciated lode, showed that Ag is the main alloying component, varying from 0.3 to 11.2%, and averaging 6.0% (Table 2). Backscattered-electron imaging of gold grains shows goethite, kaolinite, tourmaline, muscovite, scorodite and an As-bearing, florencite-like phase, either on the surface or as inclusions in gold grains (Fig. 3a, b).

Tourmaline classification and major-element variations

Seventy-five electron-probe microanalyses were performed on 38 tourmaline grains (Fig. 4 and ESM Fig. 1). Average values are 32.3% Al_2O_3, 7.9% MgO, 4.7% FeO, 1.9% Na_2O and 0.5% CaO (Table 1 and Supplementary Table S1). Most microanalyses correspond to dravite, but some plot in the compositional fields of schorl and Mg-foitite in Fig. 5a. Such Fe-rich compositions mainly represent schorl-richer rim zones overgrowing dravite cores. In general, tourmaline grains show no compositional zoning. Where found, tourmaline zonation is evident in sections parallel to the c-axis. All microanalyses form an array along the dravite–Mg-foitite compositional trend in the plot Al vs. X-site vacancy (Fig. 5b). The rims compose an array along the schorl–dravite trend, while the core compositions of grains with and without rims are roughly parallel to the $AlO(Mg(OH))_{-1}$ exchange vector, extending from about 6.0 to 6.4 apfu Al, offset from the "oxy-dravite"–povondraite trend (Fig. 5c).

Boron isotopic composition of tourmaline

Sixty-five spot analyses performed on 35 tourmaline grains (Fig. 4 and ESM Fig. 1) gave $\delta^{11}B$ values between -21.3 ± 0.2‰ and -8.8 ± 1.3‰ (Table 1 and Supplementary Table S1). The $\delta^{11}B$ data have an average value of −14‰ and 89% of the data are between −16‰ and −10‰ $\delta^{11}B$, without any obvious correlation with tourmaline chemical composition (Fig. 5d). Several spot analyses on core and rim domains of single tourmaline grains returned $\delta^{11}B$ values that are either indistinguishable within error (Fig. 4, grain 10, with about −15‰ $\delta^{11}B$), or marginally close to each other. They include core domains that are isotopically heavier than their rims (Fig. 4, grain 12, with -15.0 ± 0.4‰ $\delta^{11}B$ and -17.4 ± 0.4‰ $\delta^{11}B$ for core and rim, respectively), as well as isotopically lighter core but heavier rim (Fig. 4, grain 30, with -19.1 ± 1.7‰ $\delta^{11}B$ for its core and two rim spots of -14.0 ± 1.2‰ $\delta^{11}B$ and -14.9 ± 1.9‰ $\delta^{11}B$). There are, however, tourmaline grains that are distinctly heterogeneous isotopically, for which the maximum core–rim difference of $\delta^{11}B$ values is 6‰ – i.e., Fig. 4, grain 50, whose core domains show values of -15.2 ± 0.2‰ $\delta^{11}B$ and -15.6 ± 0.2‰ $\delta^{11}B$, whereas a rim domain has the lightest value of the data set, -21.3 ± 0.2‰ $\delta^{11}B$ (Supplementary Table S1).

Discussion

The Veloso lode is highly oxidised, as expressed by goethite-rich pockets that typically have boxwork fabrics. Little is preserved from the primary sulfide mineralogy, apart from rarely observed arsenopyrite and pyrite. It is inferred from the occurrence of scorodite that arsenopyrite was locally abundant prior to oxidative weathering. In this regard, Veloso is envisaged as a secondary, weathered equivalent of the Passagem arsenopyrite–tourmaline assemblage, but hosted in itabirite and lacking easily recognisable tourmaline. In fact, the Veloso tourmaline is concentrated in the

Table 2 Electron-microprobe analyses of gold grains from the Veloso lode

Gold grain	1	2	3	4	5	6	7	8	8	9	9
Spot location	–	–	–	–	–	–	–	Rim	Core	Rim	Core
Au (%)	95.07	95.09	94.83	94.09	94.24	98.92	93.88	92.56	93.51	88.27	89.40
Ag	4.38	4.98	4.04	5.45	5.41	0.33	5.87	6.91	6.07	11.18	9.89
S	0.01	0.02	0.03	< 0.01	< 0.01	0.01	< 0.01	< 0.01	< 0.01	0.01	< 0.01
Fe	< 0.05	< 0.05	0.05	< 0.05	< 0.05	< 0.05	< 0.05	< 0.05	< 0.05	< 0.05	< 0.05
Cd	0.06	0.05	< 0.04	0.08	0.09	0.05	0.10	0.09	0.07	0.10	0.09	0.09
Sb	< 0.03	0.03	< 0.03	< 0.03	< 0.03	< 0.03	< 0.03	< 0.03	< 0.03	< 0.03	< 0.03	< 0.03
Hg	< 0.30	< 0.30	< 0.30	< 0.30	0.30	< 0.30	< 0.30	< 0.30	< 0.30	< 0.30	< 0.30	< 0.30
Bi	0.36	0.40	0.35	0.26	0.36	0.36	0.30	0.36	0.38	0.39	0.37	0.34
Total	99.94	100.65	99.38	99.99	100.45	99.99	100.41	100.25	100.51	99.97	100.24	99.96

Measurements for the following elements were performed, but their concentrations are below the minimum limit of detection: O (< 0.27%), Mn (< 0.04%), Co (< 0.05%), Ni (< 0.05%), Cu (< 0.05%), As (< 0.15%), Se (< 0.06%), Mo (< 0.04%), Sn (< 0.04%), Te (< 0.04%), Pt (< 0.10%) and Pd (< 0.03%)

black, goethite-rich groundmass that cements breccia fragments of vein quartz (Fig. 3c).

The lode brecciation and the oxidative overprint further distinguish Veloso from Passagem de Mariana. The brittle rupturing of Veloso is an indication of late- to post-orogenic timing, perhaps during orogenic collapse, as envisaged by Chauvet et al. (2001). Alternatively, Veloso may represent shallow, brittle overprint on an orogenic lode-gold deposit. Lacourt (1937) noted that post-tectonic cataclastic deformation affected the auriferous lodes of the Ouro Preto area, indicating that "fracturing facilitated the oxidation of sulfides (arsenopyrite predominating over pyrite), liberating part of the gold" (Lacourt 1937, p. 92). Here, it is instructive to draw attention to the occurrence of microfractures in the Passagem de Mariana lode, where gold, maldonite and aurostibite occur in vein arsenopyrite (Chauvet et al. 2001). This observation led Oberthür and Weiser (2008) to propose an epithermal-like overprint on an otherwise mesothermal (orogenic) gold lode.

Veloso and Passagem de Mariana show a similar range of tourmaline $\delta^{11}B$ values (Fig. 6a,b). Furthermore, the deposits are located in the same structure – i.e., the southern flank of the Mariana anticline (Fig. 1). These lines of evidence suggest a common origin of B in the lode-forming fluids of both deposits. An essential factor for the formation of tourmaline is the availability of B in the system. Boron can originate from different sources in the crust and $\delta^{11}B$ values can help to resolve its origin (Fig. 6a). The Veloso $\delta^{11}B$ values are in the range of –21‰ to –9‰, with an average value of –14‰ $\delta^{11}B$ (Fig. 6b). This range rules out a marine origin for the tourmaline B, but the average $\delta^{11}B$ values are compatible with magmatic B. A direct connection of B to magmatism would be expressed as tourmaline of magmatic origin, which is compositionally characterised by high contents of Fe, Al (replacing divalent cations) and F (e.g., London and Manning 1995). The Veloso tourmaline is essentially dravite, a few compositions of which are marginally schorl (Fig. 5a), and consequently does not support a magmatic origin. Although a magmatic B source cannot entirely be excluded, a more plausible B reservoir are metasedimentary rocks, as discussed below.

Considering the metasedimentary sequence and the range of $\delta^{11}B$ values obtained from tourmaline during this and previous studies (Fig. 6a; Cabral et al. 2017; Trumbull et al. 2019), it is apparent that the majority of its B was sourced from clastic metasedimentary rocks. This interpretation is supported by 92% of the data, the $\delta^{11}B$ values of which are concentrated between −16‰ and −8‰ $\delta^{11}B$. The lightest $\delta^{11}B$ values found in the Quadrilátero Ferrífero, including those from the Veloso lode, are beyond those commonly reported from clastic metasedimentary rocks (Fig. 6a). The lightest $\delta^{11}B$ values may suggest that an additional source

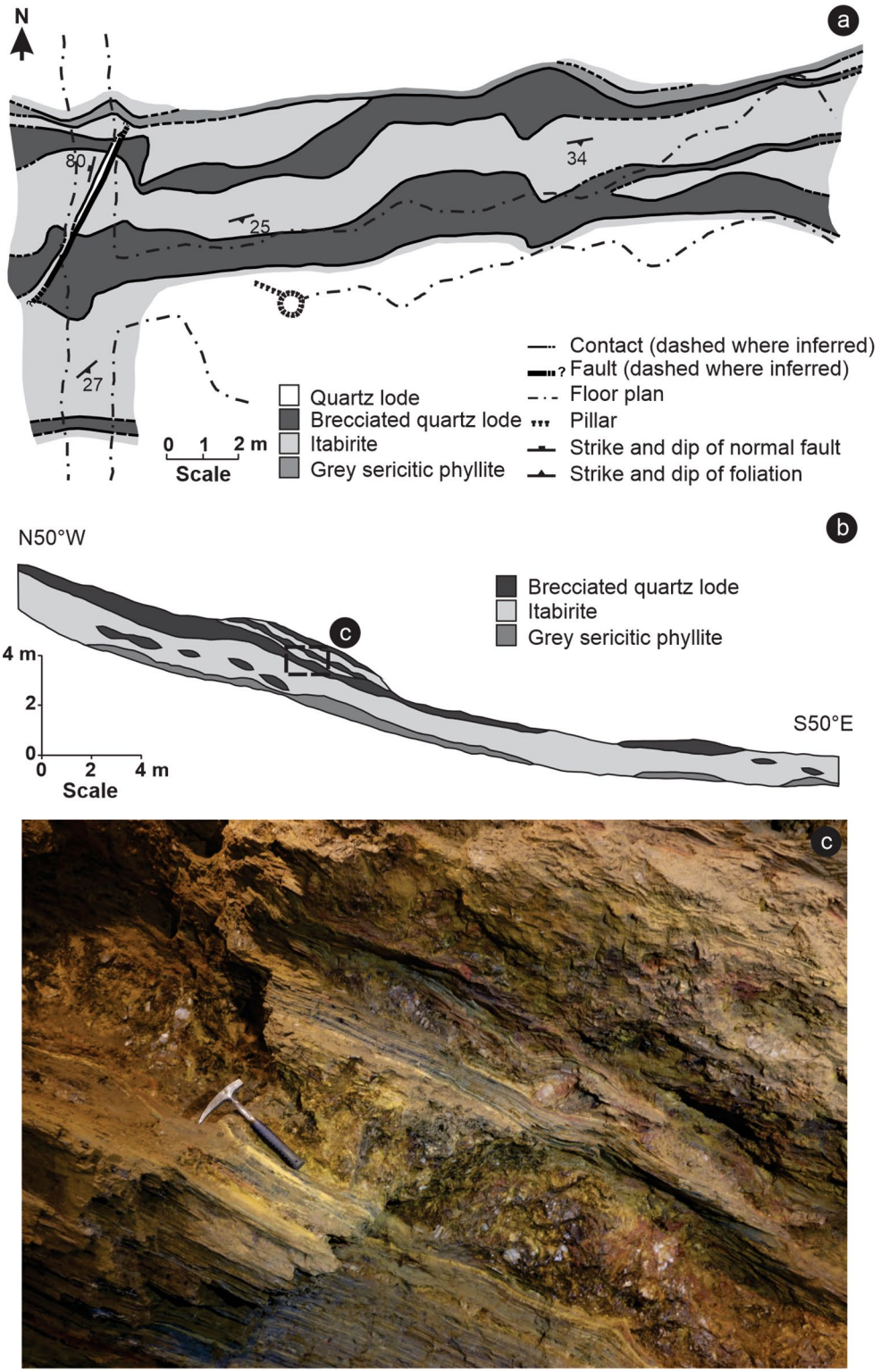

Fig. 2 **a** Geological map, projected onto a horizontal plane set at 2 m above the floor, showing where the main adit intercepts the brecciated quartz lode of the Veloso mine. **b** Geological cross-section of the Veloso lode. **c** Photograph, looking NE, of the auriferous quartz lode. Note the foliated host rock, itabirite, and the rough surface of the brecciated quartz lode where quartz clasts appear white

was involved – i.e., continental evaporitic rocks, the $\delta^{11}B$ range of which encompasses that of clastic metasedimentary rocks (Fig. 6a).

Before discussing further an additional B source, one needs to take into account that B isotopic fractionation can occur under greenschist-facies metamorphic conditions (e.g., Meyer et al. 2008; Marschall et al. 2009; Büttner et al. 2016), which affected the Mariana anticline (Herz 1978). As the Passagem de Mariana lode and the Veloso lode truncate the foliation of the host rock at low angle, both lodes

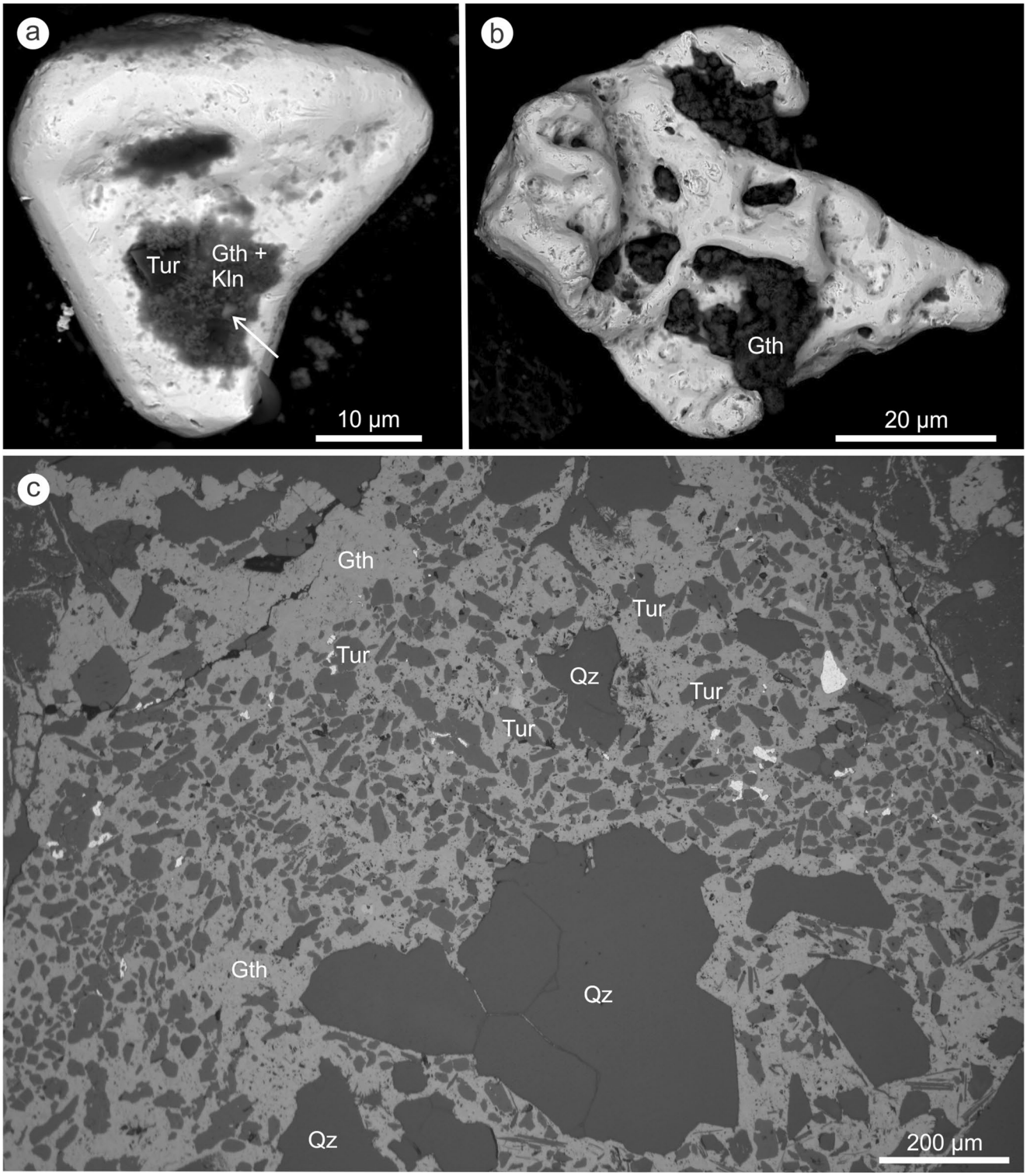

Fig. 3 **a**, **b** Backscattered-electron images of two gold grains (white), recovered from a heavy-mineral concentrate of the brecciated quartz lode of Veloso. **a** Gold grain with a partially exposed tourmaline (Tur) inclusion and a coating of goethite–kaolinite (Gth + Kln) with a scorodite-like mineral (arrow). **b** Gold grain is locally coated with goethite (Gth). **c** Reflected-light photomicrograph of a dark pocket from the brecciated quartz lode of Veloso. The dark pocket cements coarse-grained fragments of lode quartz (Qz, dark grey). The cement consists of a groundmass of goethite (Gth, light grey), where abundant tourmaline (Tur, medium grey) is dispersed as euhedral to subhedral crystals, < 200 µm in length, smaller than the angular fragments of lode quartz. Gold (white) occurs in the goethite groundmass in the immediate vicinity of tourmaline

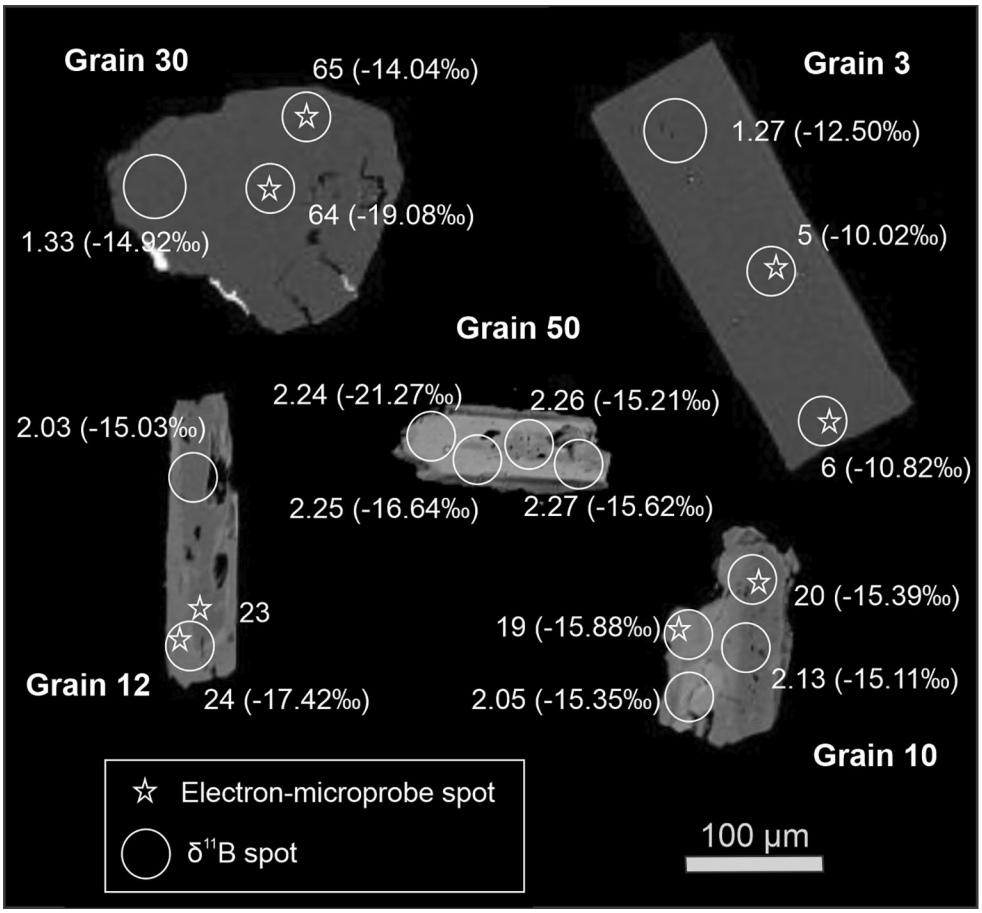

Fig. 4 Backscattered-electron image of tourmaline (light grey), embedded in resin (black). White stars represent electron-microprobe spots. Circles mark laser-ablation spots of multi-collector–ICP–MS analyses for B isotopes. Numbers correspond to individual analysis in Table 1 and Supplementary Table S1. All grains analysed in this study are documented in ESM Fig. 1

likely formed after the metamorphic peak of about 500 °C (Chauvet et al. 2001). Under such a temperature, the isotopic fractionation of B between tourmaline and aqueous fluid is about −2‰ (Meyer et al. 2008). However, two processes, Rayleigh fractionation and cooling, may account for the $\delta^{11}B$ variation of the tourmaline grain 30, from a fairly light core of -19.1 ± 1.7‰ $\delta^{11}B$ to heavier rims of -14.0 ± 1.2‰ $\delta^{11}B$ and -14.9 ± 1.9‰ $\delta^{11}B$ (Fig. 4). Rayleigh fractionation results in a progressive increase in $\delta^{11}B$ values from core to rim (e.g., Meyer et al. 2008; Pal et al. 2010), while cooling would also engender tourmaline with higher $\delta^{11}B$ values (e.g., Büttner et al. 2016; Trumbull et al. 2019). Both processes explain most of the tourmaline $\delta^{11}B$ values of this study.

The lightest $\delta^{11}B$ value of the data set, -21.3 ± 0.2‰, comes from the tourmaline grain 50 (Fig. 4). This is a single value, but it is close to a tourmaline core value of -19.1 ± 1.7‰ $\delta^{11}B$ (Fig. 4, grain 30). Furthermore, other comparably light $\delta^{11}B$ values have been recorded in tourmaline from other localities in Minas Gerais (Fig. 6). Therefore, the aforementioned value cannot be regarded as a rare exception or an artefact. Given its occurrence in a tourmaline rim domain, the lightest $\delta^{11}B$ value suggests a change in the fluid B isotopic composition. Such a change could have been caused by wall-rock tourmalinisation, as proposed for the Passagem de Mariana lode (Trumbull et al. 2019), but the Veloso lode has no halo of tourmalinisation in its immediate vicinity, as currently exposed in the underground workings. Another explanation could be a different B source. In this respect, the lightest B isotopic composition of −21‰ for the Veloso tourmaline requires a fluid $\delta^{11}B$ value of about −18‰, considering a temperature of 350–400 °C, as estimated for the Passagem de Mariana lode (Chauvet et al. 2001). The fluid $\delta^{11}B$ value was calculated using the online resource of Büttner et al. (2016). Extremely negative $\delta^{11}B$ values are known from non-marine, borate-rich evaporitic rocks (Fig. 6a; Slack et al. 1989, 1993; Palmer and Slack 1989; Palmer and Helvaci 1997). Presently, there is no direct evidence for the existence of meta-evaporitic rocks in the Minas Supergroup, but some indirect evidence. Some examples are the study of Zhelezinskaia et al. (2014), applying multiple S isotopes to the Batatal Formation, the unit in which the Passagem de Mariana lode is hosted (Fundão orebody, Vial et al. 2007), and that of Cabral et al. (2021) on tourmaline in metamorphic rocks of the Cercadinho Formation at the base of Piracicaba Group, above the Itabira Group.

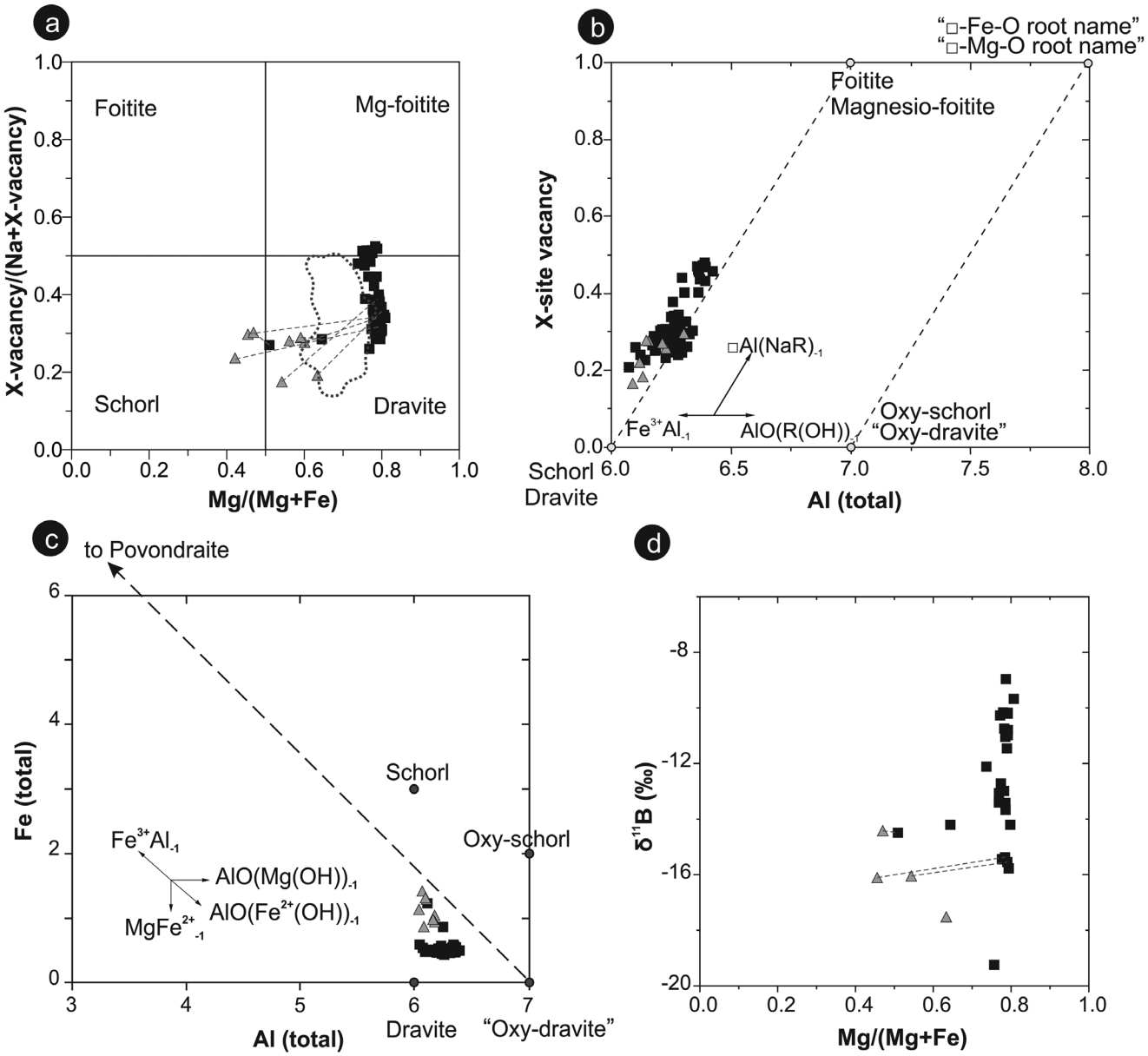

Fig. 5 Plots for tourmaline of the Veloso lode. **a** Diagram of Mg/(Mg + Fe) vs. X-vacancy/(Na + X-vacancy) for tourmaline classification (Henry et al. 2003). Dashed lines connect rim and core analyses of a single grain. The area delimited by the dotted line marks the compositional distribution of tourmaline from the Passagem de Mariana mine (compiled from the studies of Garda et al. 2009, Cavalcanti 2003, Cabral and Koglin 2012, and Trumbull et al. 2019). **b** Diagram of total Al vs. X-site vacancy, in atoms per formula unit (apfu), for tourmaline classification (Henry and Dutrow 2012). Quoted names are hypothetical tourmaline species not currently approved by the International Mineralogical Association (Henry et al. 2011). **c** Diagram of Al (total) vs. Fe (total) of Henry and Dutrow (2012). **d** Diagram of Mg/(Mg + Fe) vs. $\delta^{11}B$ values (Supplementary Table S1). Dashed lines connect rim and core microanalyses of a single grain. **a–d** Grey triangles correspond to rims of zoned crystals of tourmaline, whereas black squares refer to cores of tourmaline crystals with and without compositional zoning

Briefly, B sourced from continental evaporites seems to be a possible explanation for the fairly light $\delta^{11}B$ values (-21.3 ± 0.2‰ and -19.1 ± 1.7‰), in addition to B derived from clastic metasedimentary rocks. In any case, B was ultimately transported by crustal fluids that were also instrumental to gold mineralisation. The Veloso gold is spatially associated with locally abundant tourmaline as breccia-cementing material (Fig. 3c), pointing to a quartz-lode-overprinting fluid that is highly enriched in B. The B-rich nature of the hydrothermal fluid can also be taken as indication of an evaporitic source (e.g., Warren 2016). Conversely, the Al-rich composition of the Veloso tourmaline, from 6.1 to 6.4 apfu Al (Table 1), is remarkable because of the Al-poor nature of the brecciated-quartz-lode host

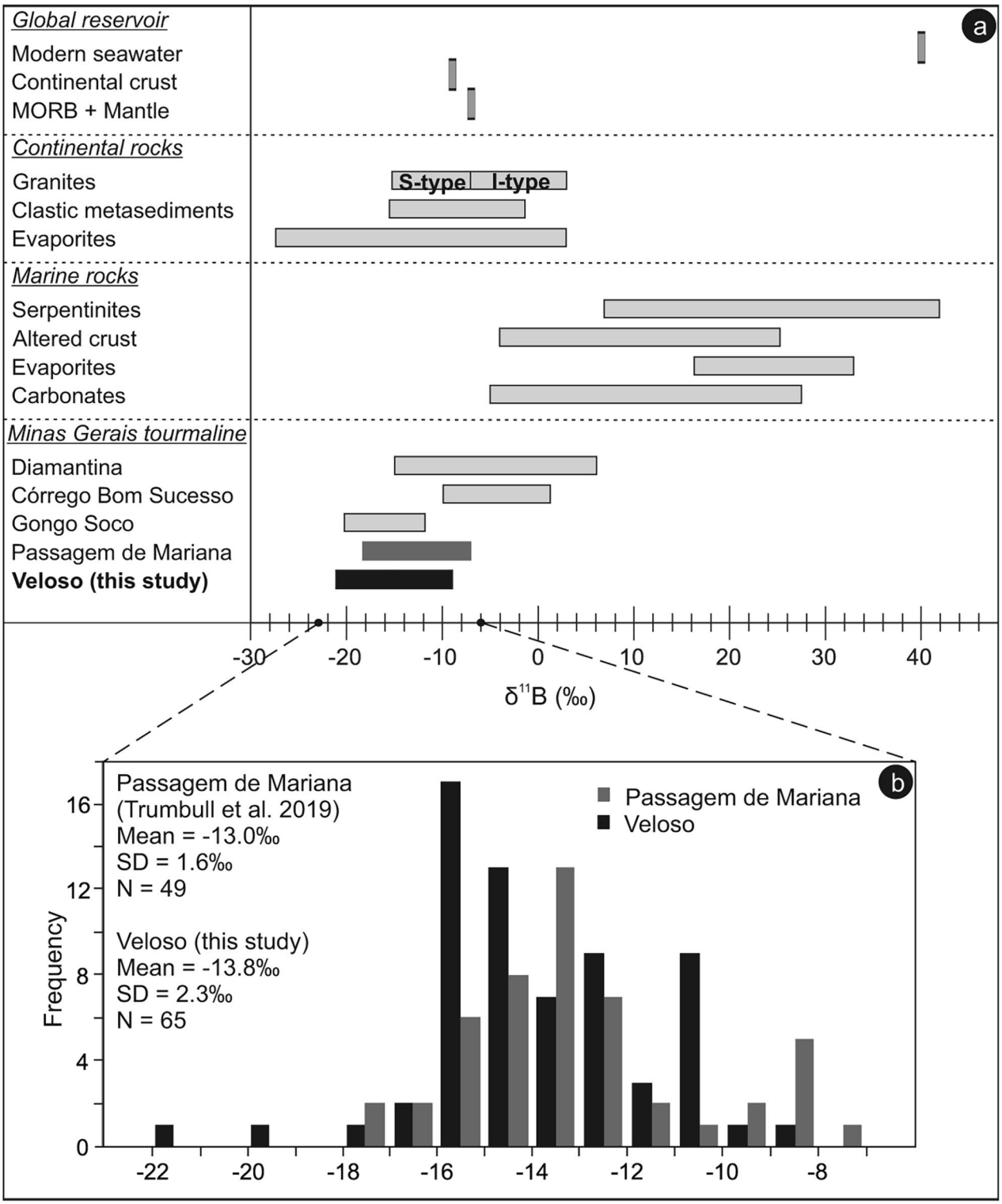

Fig. 6 **a** Comparison of B isotopic compositions for global B reservoirs, marine and continental rocks with those found in tourmaline grains from Minas Gerais (Cabral et al. 2011, 2012a, b; Trumbull et al. 2019). Data compilation for global reservoirs, continental and marine rocks is from Trumbull et al. (2019). For a temperature of 350–400 °C, as estimated for the Passagem de Mariana lode (Chauvet et al. 2001), and the lightest $\delta^{11}B$ value of –21‰ for the Veloso tourmaline, the fluid composition is about −18‰ (calculated using the online resource of Büttner et al. 2016). This isotopic composition indicates some contribution from non-marine evaporitic B (see text for discussion). **b** Frequency histogram of B isotopic ratios of the Veloso tourmaline (this study), in comparison with tourmaline from the Passagem de Mariana lode (Trumbull et al. 2019)

rock, itabirite, indicating that: (i) the tourmaline Al composition is buffered by the hydrothermal fluid (cf., Sciuba et al. 2021); (ii) its Al comes from aluminosilicate minerals. These indications not only favour B sourced from clastic metasedimentary rocks, but also B transport as aqueous aluminate-borate complexes (Tagirov et al. 2004). The formation of both aluminate-borate and gold complexes can be reconciled by devolatisation of crustal rocks, whereby Al, B and Au are part of the hydrothermal fluid from the moment it forms (Phillips 2022).

Conclusions

The finding of tourmaline in goethite-rich pockets, where arsenopyrite relicts are occasionally observed, and its characterisation as dravite connect the Veloso lode with the arsenopyrite–tourmaline (dravite) quartz lode of Passagem de Mariana, a historically and economically relevant gold deposit in the Mariana anticline. Similar signatures of tourmaline B isotopes at Veloso and at Passagem de Mariana suggest a common origin of B in the lode-forming fluids. The Veloso tourmaline, like that from Passagem de Mariana, has light $\delta^{11}B$ values, in the range of −21 to −9‰. This isotopic range for Al-rich tourmaline in the Al-poor host rock, itabirite, of the Veloso auriferous lode indicates that Al and B, and possibly Au, were sourced from metasedimentary rocks, which may include a continental evaporitic component.

Supplementary Information The online version contains supplementary material available at https://doi.org/10.1007/s00710-023-00848-9.

Acknowledgements Júlia Pimenta acknowledges a M.Sc. scholarship from FAPEMIG (13597), and Maximiliano Martins, Tiago Bastos and Rodrigo Diniz for their kind assistance during underground mapping. Diógenes S. Vial and Marco A. Fonseca shared with us their experience in underground mapping. Alexandre Lima (Universidade do Porto) generously made available polished sections of goethite-rich fragments. Additional polished sections were kindly prepared by Ulf Hemmerling and Stephanie Lohmeier at the Technische Universität Clausthal, Germany. Lucas Eustáquio Dias Amorim kindly assisted us in preparing a heavy-mineral concentrate at the CDTN. Miguel Tupinambá acknowledges CNPq for his research grant. The authors thank the Microscopy and Microanalysis Laboratory (LMic) of the UFOP, in particular Marco Paulo de Castro, for carrying out the electron-microprobe analysis of tourmaline. We acknowledge the staff of Mina Du Veloso, represented by Eduardo Evangelista Ferreira, for permission to assess and sample the underground workings. A previous version of our manuscript benefitted from the careful reading by Ferenc Molnar and Robert Trumbull, as well as comments by Fernando Tornos. They are indeed appreciated. The manuscript also improved from further reviews by Steffen Hagemann and an anonymous reviewer. Finally, we thank Steffen H. Büttner for his thoughtful review and Christoph Hauzenberger for his editorial handling. Finally, we thank the typesetting work by Junlen Fabe-Eluna.

Funding Not applicable.

Declarations

Competing interests The authors declare no competing interests.

References

Albert C, Lana C, Gerdes A, Schannor M, Narduzzi F, Queiroga G (2018) Archean magmatic-hydrothermal fluid evolution in the Quadrilátero Ferrífero (SE Brazil) documented by B isotopes (LA MC-ICPMS) in tourmaline. Chem Geol 481:95–109

Alkmim FF, Marshak S (1998) Transamazonian orogeny in the Southern São Francisco Craton region, Minas Gerais, Brazil: evidence for paleoproterozoic collision and collapse in the Quadrilátero Ferrífero. Precambrian Res 90:29–58

Babinski M, Chemale F Jr, Van Schmus WR (1995) The Pb/Pb age of the Minas Supergroup carbonate rocks, Quadrilátero Ferrífero, Brazil. Precambrian Res 72:235–245

Büttner SH, Reid W, Glodny J, Wiedenbeck M, Chuwa G, Moloto T, Gucsik A (2016) Fluid sources in the Twangiza-Namoya Gold Belt (Democratic Republic of Congo): evidence from tourmaline and fluid compositions, and from boron and Rb-Sr isotope systematics. Precambrian Res 280:161–178

Cabral AR, Koglin N (2012) Hydrothermal fluid source constrained by Co/Ni ratios in coexisting arsenopyrite and tourmaline: the auriferous lode of Passagem, Quadrilátero Ferrífero of Minas Gerais, Brazil. Min Petrol 104:137–145

Cabral AR, Zeh A (2015a) Celebrating the centenary of the Geology of Central Minas Gerais, Brazil: an insight from the Sítio Largo Amphibolite. J Geol 123:337–354

Cabral AR, Zeh A (2015b) Detrital zircon without detritus: a result of 496-Ma-old fluid-rock interaction during the gold-lode formation of Passagem, Minas Gerais, Brazil. Lithos 212–215:415–427

Cabral AR, Lehmann B, Tupinambá M, Wiedenbeck M, Brauns M (2011) Geology, mineral chemistry and tourmaline B isotopes of the Córrego Bom Sucesso area, southern Serra do Espinhaço, Minas Gerais, Brazil: implications for Au–Pd–Pt exploration in quartzitic terrain. J Geochem Explor 110:260–277

Cabral AR, Wiedenbeck M, Koglin N, Lehmann B, de Abreu FR (2012a) Boron-isotopic constraints on the petrogenesis of hematitic phyllite in the southern Serra do Espinhaço, Minas Gerais, Brazil. Lithos 140–141:224–233

Cabral AR, Wiedenbeck M, Rios FJ, Seabra Gomes AA Jr, Jones RD, Rocha Filho OG (2012b) Talc mineralisation associated with soft hematite ore, Gongo Soco deposit, Minas Gerais, Brazil: petrography, mineral chemistry and boron-isotope composition of tourmaline. Min Deposita 47:411–424

Cabral AR, Zeh A, Koglin N, Gomes AAS Jr, Viana DJ, Lehmann B (2012c) Dating the Itabira iron formation, Quadrilátero Ferrífero of Minas Gerais, Brazil, at 2.65 Ga: depositional U–Pb age of zircon from a metavolcanic layer. Precambrian Res 204–205:40–45

Cabral AR, Koglin N, Strauss H, Brätz H, Kwitko-Ribeiro R (2013) Regional sulfate–hematite–sulfide zoning in the auriferous Mariana anticline, Quadrilátero Ferrífero of Minas Gerais, Brazil. Min Deposita 48:805–816

Cabral AR, Zeh A, Galbiatti HF, Lehmann B (2015) Late Cambrian Au–Pd mineralization and Fe enrichment in the Itabira district, Minas Gerais, Brazil, at 496 Ma: constraints from U–Pb monazite dating of a jacutinga lode. Econ Geol 110:263–272

Cabral AR, Tupinambá M, Zeh A, Lehmann B, Wiedenbeck M, Brauns M, Kwitko-Ribeiro R (2017) Platiniferous gold–tourmaline aggregates in the platiniferous gold–palladium belt of Minas Gerais, Brazil: implications for regional boron metasomatism. Min Petrol 111:807–819

Cabral AR, Zeh A, Tupinambá M, Pimenta J (2020) First evidence for neoproterozoic magmatism in the Quadrilátero Ferrífero of Minas Gerais, Brazil, and geotectonic implications. J S Amer Earth Scie 104:102844

Cabral AR, DeFerreira TH, Lana C, Castro MP, Queiroga G (2021) Tourmaline composition and boron isotopes record lateritic weathering during the great oxidation event. Terra Nova 33:46–55

Cavalcanti JAD (2003) Origem dos turmalinitos auríferos da região sudeste do Quadrilátero Ferrífero-MG: evidências de campo, petrografia, química mineral e dados isotópicos de Nd e Sr. DSc. thesis, Instituto de Geociências, Universidade Estadual de Campinas, Campinas, 172 p

Cavalcanti JAD, Xavier RP (2006) Origem dos turmalinitos auríferos da região sudeste do Quadrilátero Ferrífero-MG: geologia, petrografia, química mineral e isótopos de nd. Rev Bras Geoci 36:636–647

Chauvet A, Piantone P, Barbanson L, Nehlig P, Pedroletti I (2001) Gold deposit formation during collapse tectonics: structural, mineralogical, geochronological, and fluid inclusion constraints in the Ouro Preto gold mines, Quadrilátero Ferrífero, Brazil. Econ Geol 96:25–48

Chemale F Jr, Rosière CA, Endo I (1994) The tectonic evolution of the Quadrilátero Ferrífero, Minas Gerais, Brazil. Precambrian Res 65:25–54

Derby OA (1911) On the mineralization of the gold-bearing lode of Passagem, Minas Gerais, Brazil. Am J Sci 32:185–190

Dorr JVN (1969) Physiographic, stratigraphic and structural development of the Quadrilátero Ferrífero, Minas Gerais, Brazil. US Geol Surv Prof Pap 641-A

Dyar MD, Wiedenbeck M, Robertson D, Cross LR, Delaney JS, Ferguson K, Francis CA, Grew ES, Guidotti CV, Hervig RL, Hughes JM, Husler J, Leeman W, McGuire AV, Rhede D, Rothe H, Paul RL, Richards I, Yates M (2001) Reference minerals for microanalysis of light elements. Geostand Newslett 25:441–463

Emmons WH (1940) The principles of Economic Geology. McGraw-Hill Book Company, New York, p 539

Ferrand P (1894) L'Or a Minas Geraes (Brésil). Imprensa Official do Estado de Minas Geraes, Ouro Preto

Fleischer R, Routhier P (1973) The consanguineous origin of a tourmaline-bearing gold deposit: Passagem De Mariana (Brazil). Econ Geol 68:11–22

Garda GM, Schorscher JHD, Beljavskis P, Mansueto MS, Navarro MS, Mota AA (2009) Composição química Da turmalina de turmalinitos estratiformes da mina de passagem de Mariana, sudeste do Quadrilátero Ferrífero (MG). Revista do Instituto De Geociências – USP 9(2):3–22

Gonçalves GO, Lana C, Buick IS, Alkmim FF, Scholz R, Queiroga G (2019) Twenty million years of postorogenic fluid production and hydrothermal mineralization across the external Araçuaí orogeny and adjacent São Francisco Craton, SE Brazil. Lithos 342–343:557–572

Groves DI, Goldfarb RJ, Gebre-Mariam M, Hagemann SG, Robert F (1998) Orogenic gold deposits: a proposed classification in the context of their crustal distribution and relationship to other gold deposit types. Ore Geol Rev 13:7–27

Harder EC, Chamberlin RT (1915) The geology of central Minas Gerais, Brazil. J Geol 23:341–378

Henry DJ, Dutrow BL (2012) Tourmaline at diagenetic to low-grade metamorphic conditions: its petrologic applicability. Lithos 154:16–32

Henry DJ, Dutrow BL, Selverstone J (2003) Compositional asymmetry in replacement tourmaline – an example from the Tauern Window, Eastern Alps. Am Mineral 88:1399

Henry DJ, Novák M, Hawthorne FC, Ertl A, Dutrow BL, Uher P, Pezzotta F (2011) Nomenclature of the tourmaline-supergroup minerals. Am Mineral 96:895–913

Herz N (1978) Metamorphic rocks of the Quadrilátero Ferrífero, Minas Gerais, Brazil. US Geol Surv Prof Pap 641–C:1–81

Hippertt J, Davis B (2000) Dome emplacement and formation of kilometre-scale synclines in a granite–greenstone terrain (Quadrilátero Ferrífero, southeastern Brazil). Precambrian Res 102:99–121

Hussak E (1898) Der goldführende, Kiesige Quarzlagergang Von Passagem in Minas Geraes, Brasilien. Zprakt Geol 5:345–357

Lacourt F (1937) Jazidas auriferas de Ouro Preto E Marianna, Estado De Minas Geraes – II, Minas De Santo Antonio, Camargos, Maquiné. Min Metall 2:87–95 Taquara Queimada, Sumidouro, Furquim, Cibrão, Ouro Preto, Antonio Pereira, Tapera, Ajuda, Lavras Novas, Venda do Campo, Falcão, Morro do Bule e Pinheiros

Ladeira EA (1988) Metalogenia dos depósitos de ouro do Quadrilátero Ferrífero, Minas Gerais. In: Schobbenhaus C, Coelho CES (eds) Principais Depósitos Minerais do Brasil, Brasilia DNPM/CVRD 3:301–375

Leeman WP, Tonarini S (2001) Boron isotopic analysis of proposed borosilicate mineral reference samples. Geostand Newslett 25:399–403

Lindgren W (1933) Mineral deposits. McGraw-Hill Book Company, New York, p 941

London D, Manning DAC (1995) Chemical variation and significance of tourmaline from Southwest England. Econ Geol 90:495–519

Marschall HR, Meyer C, Wunder B, Ludwig T, Heinrich W (2009) Experimental boron isotope fractionation between tourmaline and fluid: confirmation from in situ analyses by secondary ion mass spectrometry and from Rayleigh fractionation modelling. Contrib Mineral Petrol 158:675–681

Mercadier J, Richard A, Cathelineau M (2012) Boron- and magnesium-rich marine brines at the origin of giant unconformity-related uranium deposits: $\delta^{11}B$ evidence from Mg-tourmalines. Geology 40(3):231–234

Meyer C, Wunder B, Meixner A, Romer RL, Heinrich W (2008) Boron-isotope fractionation between tourmaline and fluid: an experimental re-investigation. Contrib Mineral Petrol 156:259–267

Oberthür T, Weiser TW (2008) Gold-bismuth-telluride-sulphide assemblages at the viceroy mine, Harare-Bindura-Shamva greenstone belt, Zimbabwe. Mineral Mag 72:953–970

Pal DC, Trumbull RB, Wiedenbeck M (2010) Chemical and boron isotope compositions of tourmaline from the Jaduguda U (-Cu-Fe) deposit, Singhbhum shear zone, India: implications for the sources and evolution of mineralizing fluids. Chem Geol 277:245–260

Palmer MR, Helvaci C (1997) The boron isotope geochemistry of the neogene borate deposits of western Turkey. Geochim Cosmochim Acta 61:3161–3169

Palmer MR, Slack JF (1989) Boron isotopic composition of tourmaline from massive sulphide deposits and tourmalinites. Contrib Mineral Petrol 103:434–451

Pereira I, Storey C, Darling J, Lana C, Alkmim AR (2019) Two billion years of evolution enclosed in hydrothermal rutile: recycling of the São Francisco Craton Crust and constraints on gold remobilisation processes. Gondwana Res 68:69–92

Phillips N (2022) Formation of gold deposits. Springer, Singapore, p 291

Rosière CA, Siemes H, Quade H, Brokmeier H-G, Jansen EM (2001) Microstructures, textures and deformation mechanisms in hematite. J Struct Geol 23:1429–1440

Sciuba M, Beaudoin G, Makvandi S (2021) Chemical composition of tourmaline in orogenic gold deposits. Min Deposita 56:537–560

Slack JF, Palmer MR, Stevens BPJ (1989) Boron isotope evidence for the involvement of non-marine evaporates in the origin of the Broken Hill ore deposits. Nature 342:913–916

Slack JF, Palmer MR, Stevens BPJ, Barnes RG (1993) Origin and significance of tourmaline-rich rocks in the Broken Hill district, Australia. Econ Geol 88:505–541

Tagirov B, Schott J, Harrichoury J-C, Escalier J (2004) Experimental study of the stability of aluminate-borate complexes in hydrothermal solutions. Geochim Cosmochim Acta 68:1333–1345

Tonarini S, Pennisi M, Adorni-Braccesi A, Dini A, Ferrara G, Gonfiantini R, Wiedenbeck M, Gröning M (2003) Intercomparison of boron isotope and concentration measurements. Part I: Seletion, preparation and homogeneity tests of the intercomparison materials. Geostand Newslett 27:21–39

Trumbull RB, Slack JF, Krienitz M-S, Belkin HE, Wiedenbeck M (2011) Fluid sources and metallogenesis in the Blackbird Co–Cu–Au–Bi– Y–REE district, Idaho, U.S.A.: insights from major-element and boron isotopic compositions of tourmaline. Can Mineral 49:225–244

Trumbull RB, Garda GM, Xavier RP, Cavalcanti JAD, Codeço MS (2019) Tourmaline in the Passagem De Mariana gold deposit (Brazil) revisited: major-element, trace-element and B-isotope constraints on metallogenesis. Min Deposita 54:395–414

Vial DS, Duarte BP, Fuzikawa K, Vieira MBH (2007) An epigenetic origin for the Passagem De Mariana gold deposit, Quadrilátero Ferrífero, Minas Gerais, Brazil. Ore Geol Rev 32:596–613

von Eschwege WL (1833) Pluto brasiliensis. G Reimer, Berlin, p 622

Wallace RM (1965) Geology and mineral resources of the Pico De Itabirito district, Minas Gerais, Brazil. US Geol Surv Prof Pap 341-F

Warren JK (2016) Meta-evaporites. In: Evaporites. Springer, Cham, pp 1375–1468

Whitney DL, Evans BW (2010) Abbreviations for names of rock-forming minerals. Am Min 95:185–187

Zhelezinskaia I, Kaufman AJ, Farquhar J, Cliff J (2014) Large sulfur isotope fractionations associated with Neoarchean microbial sulfate reduction. Science 346:742–744